The Canadian Mineralogist
Vol. 44, pp. 693-714 (2006)

A LA–ICP–MS EVALUATION OF Zr RESERVOIRS IN COMMON CRUSTAL ROCKS: IMPLICATIONS FOR Zr AND Hf GEOCHEMISTRY, AND ZIRCON-FORMING PROCESSES

FERNANDO BEA[§], PILAR MONTERO AND MIGUEL ORTEGA

Department of Mineralogy and Petrology, Campus Fuentenueva, University of Granada, E–18002 Granada, Spain

ABSTRACT

The results of ~4000 LA–ICP–MS analyses in 152 thin sections from common crustal rocks reveal that several rock-forming minerals contain tens to a few thousand ppm of Zr. The highest concentrations of Zr are found in xenotime, followed by titanite, ilmenite, rutile, allanite, amphibole, clinopyroxene, garnet, magnetite and, less commonly, plagioclase, K-feldspar and orthopyroxene. Olivine, cordierite, biotite, muscovite, apatite, epidote and monazite have low levels of Zr (<5 ppm, generally <1 ppm). The minerals with the highest K_D^{Hf}/K_D^{Zr} are titanite (2.5), orthopyroxene (2.0), amphibole and clinopyroxene (1.8), and epidote and rutile (1.6–1.7). Ilmenite, magnetite, the feldspars and apatite have $K_D^{Hf}/K_D^{Zr} \approx 1$, and values less than one were found in xenotime and zircon (0.8), garnet (0.7), and allanite (0.6). The most important implications of these results follow. First, the growth of a Zr-bearing phase during partial melting does not influence the Zr concentration of the melt, but increases the fraction of zircon that can be dissolved at a given temperature. This accelerates the disappearance of zircon from the protolith or, in melts already segregated, the dissolution of inherited zircon. The effect will be more marked in metaluminous magmas precipitating amphibole and titanite than in any other type of magma. Second, the presence of Zr-bearing phases has little influence of the zircon-saturation "geothermometer". It may cause somewhat higher (20–30°C) results in metaluminous rocks, but has no effect on peraluminous rocks. Third, the uptake of Zr by major minerals in crystallizing magmas may reduce both the concentration of Zr in the melt available to form zircon and the temperature at which zircon begins to precipitate. Mineral–melt reactions involving Zr-bearing phases may lead to zircon grains with complicated patterns of zoning and texturally discordant zones, apparently diachronous. Fourth, higher-than-chondrite Zr/Hf fractionates may arise from titanite, amphibole or clinopyroxene fractionation, but this requires very little or no crystallization of zircon. Significantly lower-than-chondrite Zr/Hf magmas only result from zircon fractionation. Lastly, two new examples of mineral reactions that involve the formation of a mass-balancing accessory phase, useful for high-resolution geochronology, are described: the formation of xenotime as a product of the breakdown of garnet in amphibolite-grade metapelites, and the subsolidus growth of a new rim on zircon included in Zr-bearing feldspars.

Keywords: zircon, xenotime, mineral composition, saturation temperature, Zr, Zr/Hf, geochronology, geochemistry.

SOMMAIRE

Les résultats d'environ 4000 analyses effectuées par la technique LA–ICP–MS sur 152 lames minces de roches banales de la croûte montrent que plusieurs des minéraux formant ces roches contiennent des dizaines, voire des milliers de ppm de Zr. Les concentrations les plus élevées de Zr sont dans le xénotime, suivi de la titanite, l'ilménite, le rutile, l'allanite, l'amphibole, le clinopyroxène, le grenat, la magnétite et, moins couramment, le plagioclase, le feldspath potassique et l'orthopyroxène. L'olivine, la cordiérite, la biotite, la muscovite, l'apatite, l'épidote et la monazite possèdent de faibles teneurs en Zr (<5 ppm, et en général, <1 ppm). Les minéraux ayant les valeurs les plus élevées de K_D^{Hf}/K_D^{Zr} sont titanite (2.5), orthopyroxène (2.0), amphibole et clinopyroxène (1.8), et épidote et rutile (1.6–1.7). L'ilménite, la magnétite, les feldspaths et l'apatite possèdent une valeur K_D^{Hf}/K_D^{Zr} voisine de 1, et des valeurs inférieures sont typiques du xénotime et du zircon (0.8), du grenat (0.7), et de l'allanite (0.6). Les implications les plus importantes de ces résultats suivent. 1) La croissance d'une phase porteuse de Zr au cours de l'anatexie n'influence pas la concentration de Zr dans la fraction liquide, mais augmente la fraction de zircon qui peut dissoudre à une température donnée. Ceci a pour effet d'accélérer la disparition du zircon du protolithe ou, dans un liquide déjà séparé, la dissolution du zircon hérité. Cet effet sera plus marqué dans les magmas métalumineux précipitant l'amphibole et la titanite que dans tout autre type de magma. 2) La présence de phases porteuses de Zr exerce très peu d'influence sur le "géothermomètre" fondé sur la saturation en zircon. Elle peut être la cause de températures légèrement plus élevées (20–30°C) dans les roches métalumineuses, mais n'a aucun effet dans le cas des roches hyperalumineuses. 3) L'incorporation de Zr dans les principaux minéraux cristallisant dans un magma peut réduire à la fois la concentration de Zr pour former le zircon dans le liquide et la température à laquelle le zircon commence à cristalliser. Les réactions entre minéral et liquide impliquant les phases porteuses de Zr pourraient mener à des grains de zircon ayant des tracés compliqués de zonation et à des zones discordantes,

§ *E-mail address*: fbea@ugr.es

apparemment diachrones. 4) Des valeurs de Zr/Hf plus élevées que les valeurs chondritiques peuvent résulter d'un fractionnement de titanite, d'amphibole ou de clinopyroxène, mais ceci requiert très peu (ou aucune) cristallisation de zircon. Les magmas ayant une valeur Zr/Hf plus faible que la valeur chondritique ne peuvent résulter que du fractionnement du zircon. 5) Nous décrivons deux nouveaux exemples de réactions minérales impliquant la formation d'une phase accessoire selon le bilan des masses, ce qui s'avère très utile dans le domaine de la géochronologie à résolution élevée: la formation du xénotime comme produit de déstabilisation du grenat dans les métapélites au faciès amphibolite, et la surcroissance subsolidus sur les grains de zircon inclus dans un feldspath porteur de Zr.

(Traduit par la Rédaction)

Mots-clés: zircon, xénotime, composition des minéraux, température de saturation, Zr, Zr/Hf, géochronologie, géochimie.

Introduction

The importance of the geochemistry of zirconium and hafnium, the companion element of Zr, invariably camouflaged in Zr minerals owing to its lower abundance and almost identical ionic radius, stems from two facts. First, Zr is an essential structural component of zircon ($ZrSiO_4$), a ubiquitous accessory phase with outstanding petrogenetic and geochronological applications (Hanchar & Hoskin 2003). Second, Zr and Hf concentrations and the ratio Zr/Hf find application as indicators of magmatic and metallogenetic processes (*e.g.,* Linnen 1998, David *et al.* 2000, Kamber & Collerson 2000).

Background Information

In this paper, we present the most relevant results of a survey to determine the concentration of Zr and Hf in rock-forming minerals of common crustal rocks. We first summarize results of about 4000 analyses from 152 thin sections of a wide variety of igneous and metamorphic rocks from Iberia, the Urals, the Alps and the Kola Peninsula, and of about 500 analyses of zircon grains from mineral concentrates from a representative selection of these samples. We then discuss how the presence of Zr-bearing minerals may affect the zircon saturation in magmas and, therefore, zircon inheritance and crystallization, and the evolution of Zr/Hf during magmatic differentiation. The potential of breakdown reactions of Zr-bearing minerals to produce new zircon (or any other accessory phase) useful for geochronology is also considered.

There are 99 known Zr minerals: 73 silicates, 14 oxides, six phosphates, three borates and three carbonates (see http://www.MinDat.org/index.php), but most of them are restricted to peralkaline silica-undersaturated and -oversaturated rocks, which are volumetrically insignificant at a crustal scale. In the great majority of common crustal rocks, from metapelites, gneisses and granitic rock to eclogites, ophiolites and alkali basalts, the only primary Zr minerals are zircon (by far the most abundant), baddeleyite (ZrO_2, restricted to olivine-normative rocks including members of calc-alkaline and tholeiitic suites) and zirconolite–zirkelite ($CaZrTi_2O_7$ – $[Ca,Th,Ce]Zr[Ti,Nb]_2O_7$, restricted to nepheline-normative rocks). But these minerals are not the only repositories of Zr; several silicates and oxides have also been found to contain small but significant concentrations of this element (*e.g.,* Pearce 1990, Fraser *et al.* 1997, Vannucci *et al.* 1998, Seifert & Kramer 2003). Upon breakdown, some of them may even release sufficient Zr to form new crystals of zircon (Bingen *et al.* 2001, Degeling *et al.* 2001).

The partitioning of Zr and Hf in rock-forming minerals is not yet well known, despite the profound influence it may have on the geochemistry of these elements and zircon-forming processes. Historically, this is attributable to analytical problems related with the difficulties in avoiding zircon (or xenotime, baddeleyite, *etc.*) inclusions in mineral-concentrate analysis, the lack of sensitivity of the electron microprobe, and the limited availability of ion-microprobe instruments. Now, however, these problems may be overcome with the laser-ablation inductively coupled plasma – mass spectrometry (LA–ICP–MS) technique, because it can easily perform rapid, sensitive and precise spot-analyses of Zr and Hf in minerals of rock thin-sections at a moderate cost.

Samples and Methods

Our sample collection comprises a total of 152 thin sections of representative examples of common igneous and metamorphic rocks. These include: peraluminous S-type granitic rocks (32 sections), appinitic ultramafic and mafic rocks (7), amphibolite-grade metapelites (5) and migmatites (13), and alkaline (camptonitic) lamprophyres (6) from central Spain; calc-alkaline granitic rocks (32), ophiolitic gabbros and ultramafic rocks (12), amphibolites (3) and eclogites (4) from the Urals, Russia; amphibolite- to granulite-grade metapelites (14), mafic granulites (4), and peridotites (5) from the Ivrea–Verbano zone, northwestern Italy; alkaline gabbros (3), migmatites (3) and calc-alkaline gneisses (3) from Kola, Russia; and amphibolites (3) and eclogites (3) from the Betic Cordilleras, southeastern Spain. Most of these rocks are of upper Carboniferous to lower Permian age; exceptions are the middle Proterozoic migmatites and gneisses of Kola, and the Alpine

rocks of the Betic Cordilleras. Peralkaline rocks, both silica-saturated and -undersaturated, were deliberately excluded because they play a minor role in crustal evolution and have a distinct, and highly complicated, Zr geochemistry controlled by the formation of alkali zirconosilicate complexes. Such rocks will form the basis of a future study. Accordingly, the optimum fields for application of our data are subduction- and collision-related magmatism, and medium- to high-grade metamorphism and anatexis of pelites and graywackes. A table with the localities, rock name, the nature of the Zr-saturated phase, and the summary statistics for the minerals analyzed in each section, is available from the authors as a SYLK file, and was submitted to the Depository of Unpublished Data, CISTI, National Research Council of Canada, Ottawa, Ontario K1A 0S2, Canada.

Laser-ablation analyses were done on sections 60–70 μm thick; this thickness was such that the laser did not pierce the sample (under the conditions described below), but still permitted good observations under the optical microscope. Sections were studied first by optical methods and back-scattered-electron images acquired with a scanning electron microscope (BSE–SEM) to determine inclusion-free areas, subsequently analyzed by EDAX for major elements.

The laser-ablation inductively coupled plasma – mass spectrometry (LA–ICP–MS) system consisted of a torch-shielded quadrupolar Agilent–7500 spectrometer and a 213 nm Nd–YAG Mercantek laser unit. Ablation was done in a He atmosphere. The laser beam was set either at a 95-μm-sided square section or a circular section 120 μm in diameter, depending on Zr concentrations. For analysis of xenotime in garnet aureoles, the laser beam was set to 20 μm. The laser-repetition rate was 10 Hz. Spots were pre-ablated for 60 seconds using a laser output energy of 50%. Ablation lasted 60 seconds, with a laser output energy of 75%, with the sample stage moving upward 5 μm every 20 seconds to keep the laser focused and maximize the ablation efficiency. Silicon or Ca (for apatite), Ti (for rutile and ilmenite), Fe (for magnetite) or P (for xenotime and monazite), previously determined by EDAX, were used as internal standards. The glass NIST–610, which contains 415 ppm Zr and 419 ppm Hf (Pearce *et al.* 1997), was used as an external standard. Every analytical session started and ended by analyzing NIST–610, which was also measured every 6 to 8 spots. To improve detection limits, blanks (*i.e.*, analyses with the laser energy set to zero) were recorded before each spot and subtracted from the analytical signal. Data were reduced using home-made software (freely available from F. Bea) written in STATA programming language (Statacorp. 2005). This software permits outliers to be identified and discarded, blank subtraction, drift correction, correction for an internal standard and conversion to concentration units based on an external standard. The precision, calculated as the coefficient of variation (100*standard deviation/average) on 10 replicates of NIST–610 measured in every session, was about ±3% for Zr and Hf. One experiment to estimate the precision at lower levels of concentration, run with a laser beam 120 μm in diameter on two glasses prepared for this study with levels of concentration of ~1 ppm and ~0.1 ppm, yielded values of ±10% and ±17%. With the conditions described, the detection limit for Zr and Hf was about 0.05 ppm for 95-μm-squared spots, and about 0.01 ppm for circular spots 120 μm in diameter. These figures do not apply to rutile, ilmenite or magnetite analyses because the inadequacy of the NIST–610 (a borosilicate glass) as an external standard for Fe–Ti oxides, and the fact that either Fe and Ti, used as internal standards, are prone to oxide-ion isobaric interferences in the ICP–MS system. The results for these minerals can be affected by systematic errors and so should be used with caution. To prevent contamination resulting from minute inclusions of zircon, or other Zr-rich minerals, those analyses that in $^{90}Zr/^{29}Si$ *versus* time plots yielded spikes higher than three times the signal-ratio standard-deviation were discarded.

The level of Zr in zircon was determined by either electron microprobe or EDAX–SEM using the SPI® AS2230–AB (ZrO_2 79.93%, HfO_2 1.78%, Y_2O_3 18.25%) as external standard. The Zr:Hf ratio in zircon, however, was directly determined by LA–ICP–MS by measuring $^{91}Zr/^{178}Hf$ under the same conditions as before, using a home-made glass of eudialitic composition (98200 ppm Zr, 1910 ppm Hf, and Zr/Hf = 51.4) as an external standard. The precision estimated on 10 replicates measured in each run was usually better than 2%.

Zirconium Abundances in Rock-Forming Minerals

Results of LA–ICP–MS analyses of minerals are summarized in Table 1. As the frequency-distribution patterns of Zr in each mineral are commonly strongly asymmetrical, the mode is also reported in addition to the mean and the standard deviation. As Hf was found to be near or below detection limit in many instances, we report in Table 1 only the Zr/Hf mode for each mineral in each rock type. In addition, the variability in Zr/Hf is displayed by kernel-density plots (a refinement of a histogram or frequency plot) calculated with the gaussian kernel function (Statacorp. 2005). As Zr/Hf shows little or no dependence on the nature of the host rock (Table 1), only one kernel-density plot was required for each mineral. The most important observations are as follows.

Olivine

The concentration of Zr in olivine from tholeiitic gabbros and peridotites in this study is invariably below the detection limit (0.01 ppm). Olivine from alkaline

TABLE 1. SUMMARY OF THE CONCENTRATION OF Zr IN ROCK-FORMING MINERALS

Mineral	Rock type	*N*	Zr (ppm)			Hf (ppm)			Zr/Hf
			mode	*mean*	*σ*	*mode*	*mean*	*σ*	*mode*
olivine	tholeiitic gabbro and peridotite	92	b.d.l.	b.d.l.	--	b.d.l.	b.d.l.	--	--
	alkaline gabbro	12	0.05	0.06	0.05	b.d.l.	b.d.l.	--	--
	cortlandite	10	1.3	1.5	0.5	0.03	0.03	0.01	42
ortho-pyroxene	ultramafic rocks	31	0.02	0.06	0.08	b.d.l.	b.d.l.	--	--
	tholeiitic gabbro	14	1.3	3.2	3.9	0.07	0.18	0.21	19
	appinite	17	4.0	4.0	0.9	0.21	0.19	0.02	19
	mafic granulite	12	0.2	0.4	0.7	0.01	0.01	0.03	20
	felsic granulite	8	22	24	4.2	1.15	1.16	0.26	19
clino-pyroxene	ultramafic rocks	10	6.5	5.1	2.7	0.43	0.36	0.20	15
	tholeiitic gabbro	83	3.0	2.9	2.8	0.17	0.15	0.12	18
	calc-alkaline rocks	13	4.1	4.2	1.0	0.19	0.19	0.07	22
	alkali gabbro and camptonite	68	23	30.6	18.6	1.17	1.52	0.73	20
	mafic granulite	13	158	137	45	7.3	6.9	2.9	22
	eclogite	17	1.3	8.9	13	0.07	0.43	0.52	19
amphibole	tholeiitic rocks	23	7.2	8.3	3.6	0.32	0.37	0.17	23
	calc-alkaline gabbro and diorite	49	135	154	57	7.1	7.6	3.01	19
	calc-alkaline tonalite to granite	124	53	41	34	2.2	2.1	1.79	24
	appinite, Ti-rich hbl, kaersutite	34	153	163	63.5	5.7	6.3	3.26	27
	appinite, Fe-Mg amphibole	34	10.5	17	15.8	0.31	0.57	0.64	34
	camptonite, kaersutite	79	95	67	26	4.37	3.24	1.62	22
	alkaline gabbro, magnesio-arfvedsonite	20	196	187	120	10.2	10.6	6.36	19
	ultramafic rocks	16	29	28	10	1.63	1.67	0.69	18
	amphibolite	21	9.7	11.2	6.6	0.45	0.46	0.26	22
	mafic granulite	26	107	75	45	5.1	3.36	2.46	21
biotite	all rocks	397	0.65	1.84	2.23	0.05	0.17	0.19	13
muscovite	all rocks	48	0.93	1.84	1.47	0.06	0.15	0.09	16
cordierite	all rocks	169	0.03	0.29	0.56	b.d.l.	b.d.l.	--	--
garnet	peraluminous granite (24)	47	3	8.3	12.1	0.05	0.18	0.22	60
	metapelite (30)	130	12	17	16	0.29	0.35	0.35	41
	migmatite (48)	231	25	30	13	0.45	0.58	0.27	56
	felsic granulite (59)	317	33	45	21	0.67	0.85	0.44	49
	mafic granulite (28)	61	17	21	18	0.42	0.46	0.42	40
	amphibolite (22)	35	5.9	7.7	5.1	0.11	0.15	0.11	54
	eclogite (29)	72	6.2	14	13	0.16	0.28	0.30	39
plagioclase	peraluminous granite	127	3.1	9.6	14	0.08	0.31	0.44	39
	calc-alkaline granite	157	2.4	4.6	8.1	0.06	0.14	0.22	40
	appinnite	94	55	41	20	1.13	1.02	0.52	49
	tholeiitic gabbro	80	0.1	2.4	4.4	b.d.l.	b.d.l.	--	--
	metapelite	76		0.12	0.41	b.d.l.	b.d.l.	--	--
	migmatite	93	4.5	12	17	0.11	0.28	0.37	41
	felsic granulite	37	0	0.88	2.1	b.d.l.	b.d.l.	--	--
	mafic granulite	44	0.1	5.7	10		0.23	0.31	--
	amphibolite	56	0	0.05	0.07	b.d.l.	b.d.l.	--	--
K-feldspar	peraluminous granite	135	3	10.3	9.3	--	0.24	0.22	--
	calc-alkaline granite	140	11.5	10.9	9.8	--	0.25	0.19	--
	appinnite	8	27	26	3.1	0.65	0.70	0.11	42
	migmatite	45	13	18.7	11	0.38	0.44	0.28	34
	metapelite	26	0.1	0.8	1.9	b.d.l.	b.d.l.	--	--
titanite	calc-alkaline gabbro and diorite	51	1970	2023	423	130	135	33	15
	calc-alkaline tonalite to granite	74	610	893	559	43	60	40	14
	appinite	14	27	33	26	1.4	1.7	1.6	19
	alkaline gabbro, and camptonite	31	1550	2100	1310	65	80	41	24
apatite	peraluminous granite	28	4.6	11	12	0.15	0.29	0.30	31
	calc-alkaline granite	39	1.1	2.5	4.9	b.d.l.	b.d.l.	--	0
	alkaline granite	24	1.9	3.3	4.9	b.d.l.	b.d.l.	--	0
	migmatite	32	1.4	1.7	1.6	b.d.l.	b.d.l.	--	0
epidote	calc-alkaline rocks	52	4.9	6	3.5	0.25	0.30	0.20	20
monazite	peraluminous granite	19	0.8	4.5	7.3	b.d.l.	b.d.l.	--	--
rutile	felsic granulite	21	234	251	69	10.1	10.3	2.8	23
	mafic granulite	7	123	97	41	4.5	4.2	2	27
	eclogite	18	139	143	27	6.1	6.14	1.32	23
allanite	calc-alkaline rocks	11	135	272	395	2.2	4.4	7.4	61
ilmenite	calc-alkaline gabbro and diorite	4	690	677	152	19	17.1	3.7	39
	calc-alkaline tonalite to granite	5	105	127	61	2.8	3.2	1.5	40
	peraluminous granite	10	20	28	18	0.5	0.8	0.5	37
	migmatite	8	28	31	14	0.9	0.9	0.5	36
magnetite	alkali gabbro	7	50	47	21	1.3	1.2	0.5	38
	calc-alkaline granite	14	6.5	6.6	3.6	0.18	0.16	0.09	36

N represents the number of single analytical datasets computed. Except for garnet, *N* represents the number of individual crystals analyzed. For garnet, the number shown in parentheses represents the number of analyzed grains, and *N* the number of analysed spots. A table with the localities, rock name and the summary statistics for the minerals analyzed in each sections is also available (see Samples and Methods). b.d.l.: below detection limit.

basalts, however, has detectable Zr and yielded an average of 0.06 ppm (Fig. 1A). The highest concentrations of Zr (mean 1.5 ppm) were found in olivine from the Iberian cortlandites (appinitic amphibole–phlogopite peridotites). The Zr:Hf ratio, difficult to determine owing to the low concentrations of Hf, seems to be around 42 (Fig. 1B), slightly higher than the chondritic ratio of 37.1 (according to McDonough & Sun 1995).

Orthopyroxene

The concentration of Zr in orthopyroxene in this study is highly variable (Fig. 2A). The lowest values were found in Uralian harzburgites, which have a mode of 0.02 ppm and a mean of 0.06 ppm (Table 1). Tholeiitic gabbros show an asymmetrical distribution, with the mode at 1.3 ppm and the average at 3.2 ppm. As in olivine, the orthopyroxene from the Iberian cortlandites is the richest in Zr of the igneous samples, and shows a nearly symmetrical distribution, with mean and mode equal at 4.0 ppm. Orthopyroxene from mafic granulites has low concentrations of Zr, usually in the range <0.01 to 1.5 ppm. Orthopyroxene from felsic granulites, in contrast, is Zr-rich (also reported by Degeling *et al.* 2001), and yielded an asymmetrical distribution with

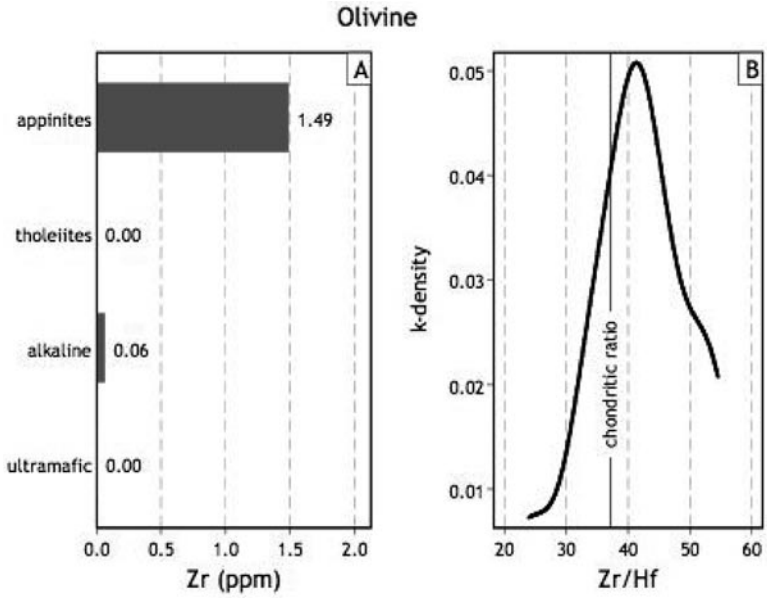

FIG. 1. A) Average concentration of Zr in olivine, sorted by rock types. Note the low but perceptible concentration in alkali basalts and the higher values in zircon in appinites. B) Kernel-density plot (see text) showing the distribution of Zr/Hf values in olivine, which shows a peak at 42; the chondritic ratio is shown at 37.1, according to McDonough & Sun (1995).

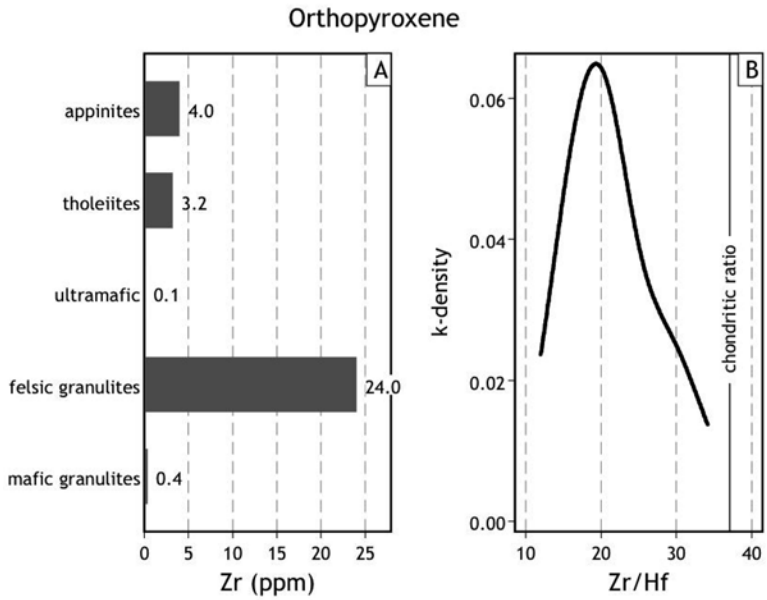

FIG. 2. A) Average concentration of Zr in orthopyroxene, sorted by rock types. The highest concentrations are found in felsic granulites. B) Distribution of Zr/Hf values in orthopyroxene. The mode is around 19, notably lower than the chondritic ratio.

the mode at 21 ppm and the mean at 24 ppm. Values of Zr/Hf in Zr-bearing orthopyroxene are systematically lower than the chondritic ratio, with the most frequent value placed around 19 (Fig. 2B).

Clinopyroxene

Clinopyroxene crystals analyzed in this study contain detectable amounts of Zr. The lowest concentrations were found in clinopyroxene from tholeiitic gabbros, which yielded a symmetrical distribution centered at 3 ppm with a mean of 2.9 ppm (Fig. 3A, Table 1). Augite from calc-alkaline gabbros yielded a similar pattern of distribution, but centered at 4.1 ppm (mean = 4.2 ppm). Chromium-rich diopside from both Uralian pyroxenites and Alpine lherzolites from Ivrea has somewhat higher Zr contents, displaying an asymmetrical distribution with the mode at 6.5 ppm and the mean at 5.1 ppm. The concentration of Zr increases notably in clinopyroxene of alkaline gabbros and lamprophyres (generally titanian augite), which has Zr in the range 8–110 ppm, with the mode at 21 ppm and the mean at 31 ppm. The distribution of Zr contents in omphacite in eclogitic rocks is asymmetrically tailed to the high end, with a mode at 1.3 ppm and the mean at 8.9 ppm. The highest concentrations of Zr were found in Mg-rich augite from the mafic granulites of the Ivrea Zone, with a mean at 137 ppm and a mode at 158 ppm. Values of Zr/Hf in clinopyroxene are notably lower than the chondritic ratio, and cluster around 21, nearly the same value as in orthopyroxene (Fig. 3B).

Amphibole

Among coexisting major minerals, amphibole commonly has the highest concentration of Zr (Fig. 4A, Table 1). In this study, the lowest values were found in edenite of tholeiitic gabbros and diabases, which show a quasi-normal distribution centered around 8 ppm (with a mean of 8.3 ppm and a mode at 7.2 ppm). Edenite to pargasite from calc-alkaline granitic rocks commonly have elevated Zr concentrations, especially in the less silicic varieties. In gabbros and diorites, these amphiboles have a mean of 154 ppm and a mode of 137 ppm, whereas in tonalites, granodiorites and granites, they yielded a mean of 41 ppm (mode = 53 ppm). Kaersutitic amphibole from appinitic cortlandites is also rich in Zr, with a mean of 163 ppm and a mode of 153 ppm. This amphibole is rimmed by a low-Ca amphibole (Bea *et al.* 1999) with much lower Zr contents (mean = 17 ppm, mode = 10.5 ppm). The kaersutite from camptonitic lamprophyres has lower Zr than in appinites, and yielded an asymmetrical distribution tailed to the low end, with a mode at 95 ppm and a mean at 67 ppm. The arfvedsonitic amphibole of alkali gabbros from Kola yielded a mean of 187 ppm and a mode of 196 ppm. The amphibole from peridotites displays an asymmetric distribution tailed to the low end, with a

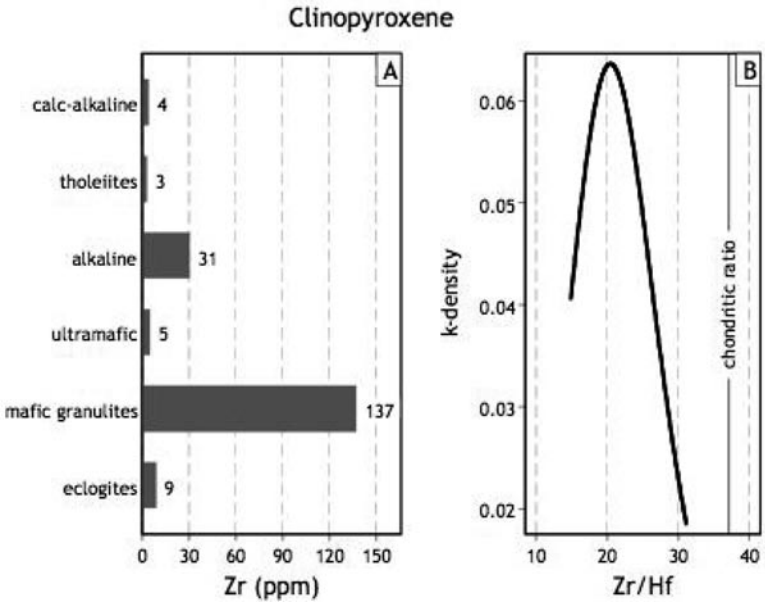

FIG. 3. A) Average concentration of Zr in clinopyroxene, sorted by rock types. The highest values are found in mafic granulites. B) Distribution of Zr/Hf values in clinopyroxene. It clusters around 20, the same value as orthopyroxene.

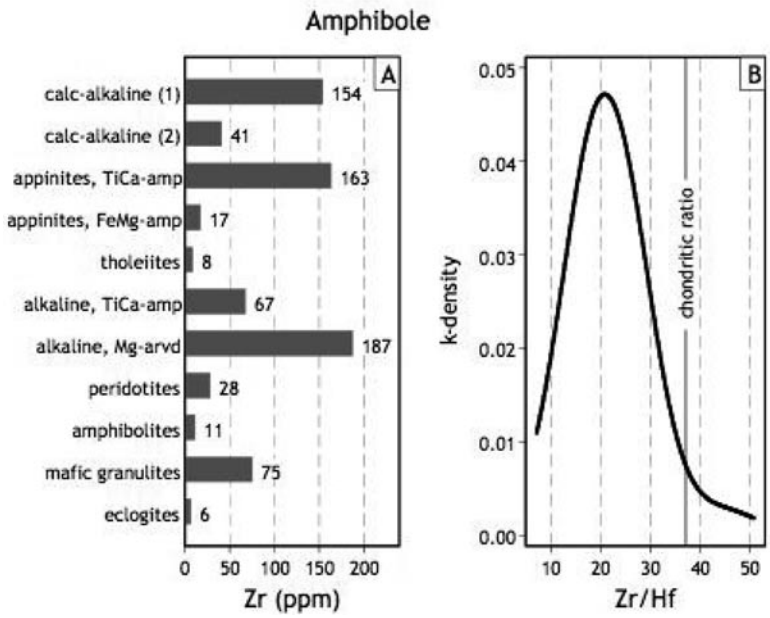

FIG. 4. A) Average concentration of Zr in amphibole, sorted by rock types. Calc-alkaline (1) represent amphibole from gabbro and diorite; calc-alkaline (2) represent amphibole from tonalite to granite. B) Distribution of Zr/Hf values in amphibole. Note that the most commonly encountered value in amphibole, Zr/Hf ≈ 20, is the same as in the two pyroxenes and notably lower than the chondritic value.

mode of 39 ppm and a mean of 28 ppm. The amphibole from amphibolites has nearly the same concentrations and patterns of distribution of Zr as that from tholeiitic gabbros. In mafic granulites, however, the Zr in amphibole may be higher, with values commonly above 100 ppm (mode = 107 ppm, mean = 75 ppm). By contrast, the amphibole from eclogites has the lowest Zr contents, yielding an asymmetrical distribution tailed to the high end, with a mode of 1.5 ppm and a mean of 6.3 ppm. The Zr/Hf value is also lower than in chondrite, with the most common value around 21, the same as the two pyroxenes (Fig. 4B).

Biotite and muscovite

The concentration of Zr in the two micas in this study is, in most cases, lower than 1 ppm and does not show perceptible variations from one rock type to another. Both show notably asymmetrical distributions tailed to the high end (Fig. 5), with modes at 0.6 ppm (biotite) and 0.9 ppm (muscovite), and equal mean values of 1.8 ppm. The Zr/Hf value in both micas is around 10, though this value should be used cautiously because Hf is generally below or near the detection limit.

Garnet

For the samples in this study, garnet invariably contains a few ppm of Zr (Fig. 6A, Table 1). In metasedimentary rocks, the lowest concentrations of Zr were found in garnet from low-grade metapelites, and the highest appear in garnet from migmatites and felsic granulites, where most values are in the range 20–80 ppm, with a mean of 45 ppm and a mode of 33 ppm. In garnet in metapelitic rocks of the Ivrea Zone, the concentration of Zr increases with the metamorphic grade (Fig. 7), whereas Y and the HREE decrease (Bea *et al*. 1997, Bea & Montero 1999). Villaseca *et al*. (2003) reported garnet grains from felsic granulites (found as xenoliths in Iberian lamprophyres) with Zr concentrations as high as 450 ppm, but we were unable to reproduce these results in the same materials from neighboring areas. Garnet of mafic granulites also contain elevated Zr contents; they yield an asymmetrical distribution, with the mode at 12 ppm and the mean at 24 ppm. In most cases, the garnet in amphibolites has low Zr, commonly in the range 0.5–3 ppm, but rarely it may contain up to several tens of ppm Zr. The distribution is highly asymmetrical, with the mode at 1.9 ppm

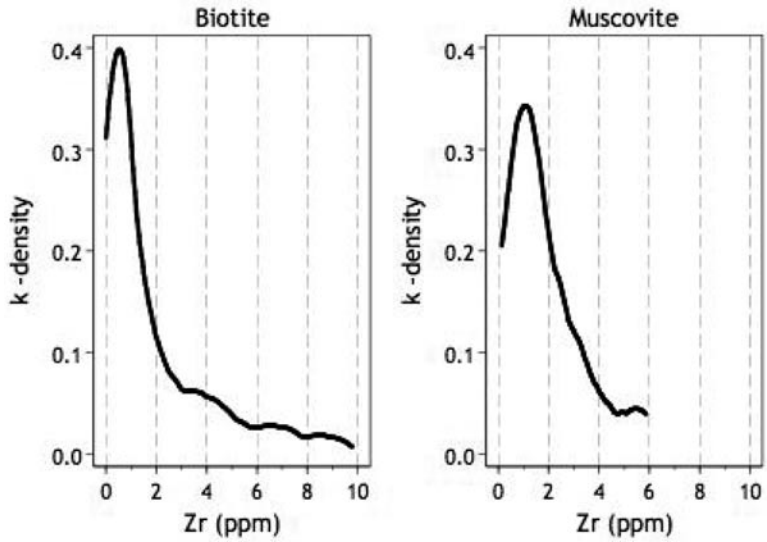

FIG. 5. Kernel-density plots of the Zr concentration in biotite and muscovite. In both cases, the mode is lower than 1 ppm. Zirconium concentrations higher than 10 ppm may be regarded as spurious, and probably caused by inclusions. Hf is below, detection limit.

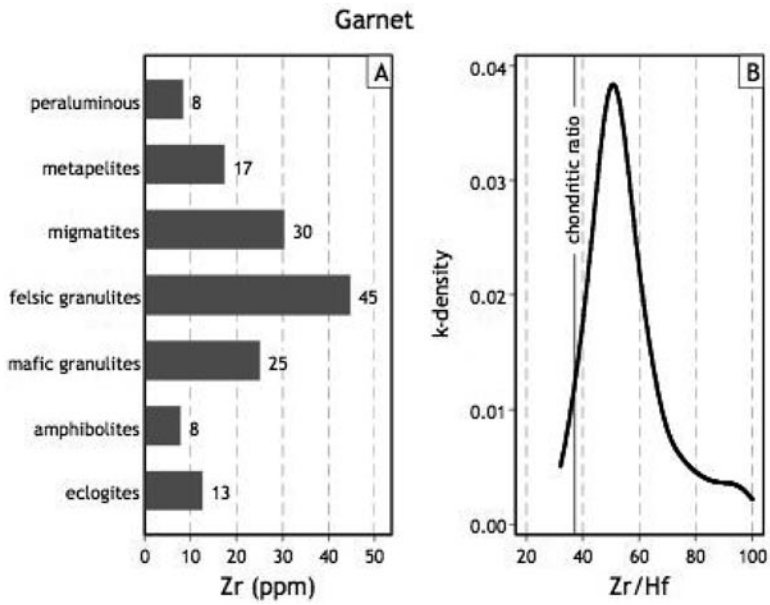

FIG. 6. A) Average concentration of Zr in garnet, sorted by rock types. B) Distribution of Zr/Hf values in garnet. Note that it is one of the few minerals with Zr/Hf higher than the value in chondrite.

and the mean at 7.7 ppm. This situation is paralleled by garnet in eclogites, but at slightly higher values, with a mode at 2.1 ppm and a mean at 12 ppm. Lastly, almandine from highly evolved peraluminous granites also shows an asymmetrical distribution, with the mode at 3 ppm and the mean at 8.3 ppm. The Zr/Hf value in garnet is higher than chondrite, and clusters around 51 (Fig. 6B).

Cordierite

Cordierite is one of the major minerals that is poorest in Zr. In this study, most values are below 0.1 ppm, with the mode at 0.03 ppm and the mean at 0.29 ppm (Table 1).

Plagioclase

Plagioclase from magmatic rocks in this study usually contains detectable, though highly variable, concentrations of Zr (Table 1, Fig. 8A). In tholeiitic gabbros, most values are close to zero, but there are also a few outliers with Zr in the range 1 to 10 ppm Zr. Something similar is observed in calc-alkaline rocks (mean = 4.6 ppm, mode = 0.4 ppm), though the frequency and the Zr contents of the outliers increase, so that crystals with 20 to 80 ppm Zr represent about 5% of the total. In peraluminous granitic rocks, the fraction of plagioclase crystals with near-zero concentrations of Zr decreases, yielding a highly asymmetrical distribution with the mode at 1.1 ppm but the mean at 10 ppm. This tendency is still more marked in plagioclase from migmatites (mode = 4.5 ppm), which commonly has concentrations higher than 20 ppm. Plagioclase from appinitic rocks, whether from cortlandite, kentallenite, appinite or tonalite, is the richest in Zr, and its frequency curve is totally different from the other rock-types; here the curve is just slightly asymmetrical, tailed to the lower end, with a mode at 55 ppm and a mean at 41 ppm. By contrast, metamorphic plagioclase has near-zero Zr; in felsic granulites, we found a few grains with ten or so ppm Zr (see also Villaseca *et al*. 2003); in mafic granulites from the Ivrea Zone, the plagioclase commonly has Zr in the range 0–5 ppm. The value of Zr/Hf in plagioclase grains having Hf > 0.1 varies between 20 and 60, with the mode at ~40, which is similar to the chondritic value (Fig. 8B).

K-feldspar

K-feldspar from the granitic and migmatitic samples examined in this study also contains detectable amounts of Zr (Table 1). That from peraluminous granites has an asymmetrical distribution tailed to the high end (Fig. 9A) with a mode at 3 ppm and a mean at 10 ppm. K-feldspar from calc-alkaline granitic rocks is richer in Zr, with equal mode and mean at about 11 ppm. The highest Zr contents are found in K-feldspar from granodiorite from appinitic suites, which has a nearly symmetrical distribution with a mode at 27 ppm and

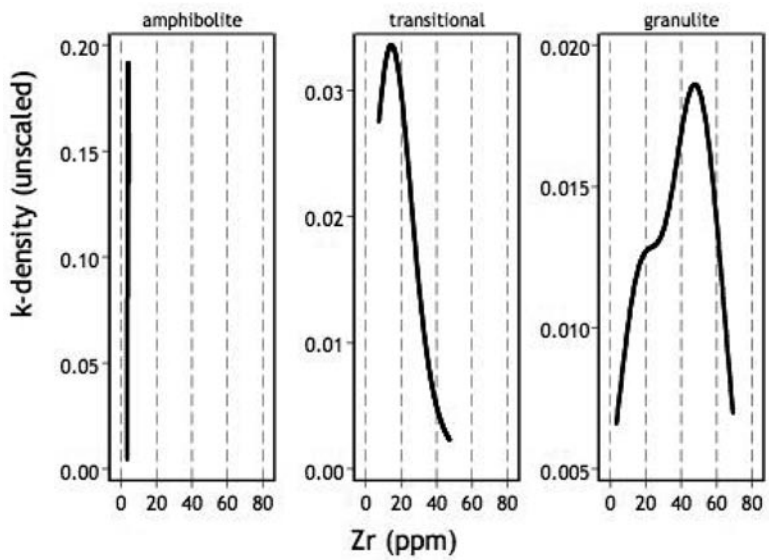

FIG. 7. Kernel-density curve of Zr contents in garnet in metapelitic rocks from the Kinzigite Formation of Ivrea–Verbano; Bea *et al*. (1997) and Bea & Montero (1999) provided descriptions of the samples. Note how the Zr contents increase with metamorphic grade.

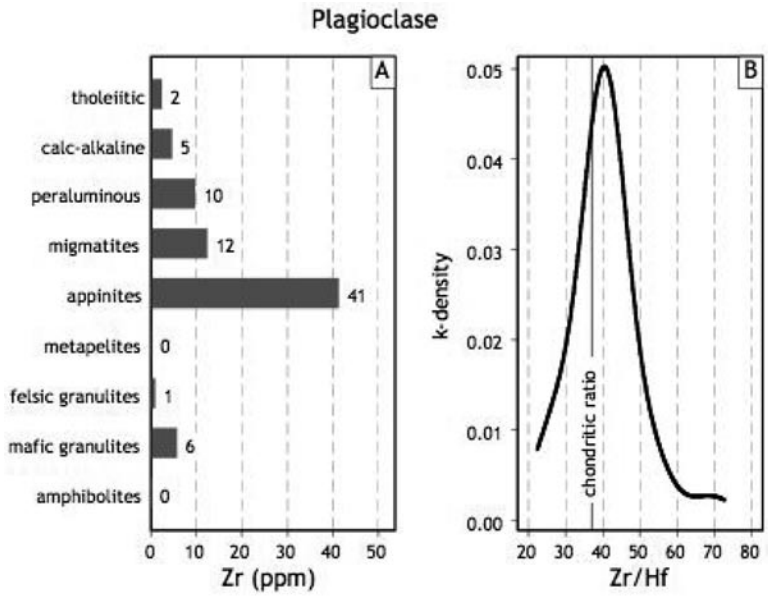

FIG. 8. A) Average concentration of Zr in plagioclase, sorted by rock types. Magmatic plagioclase usually has detectable though highly variable amounts of Zr. Compare mode and mean values in Table 1. B) Distribution of Zr/Hf values in plagioclase crystals with Hf above 0.1%. Note that it coincides with the chondritic value.

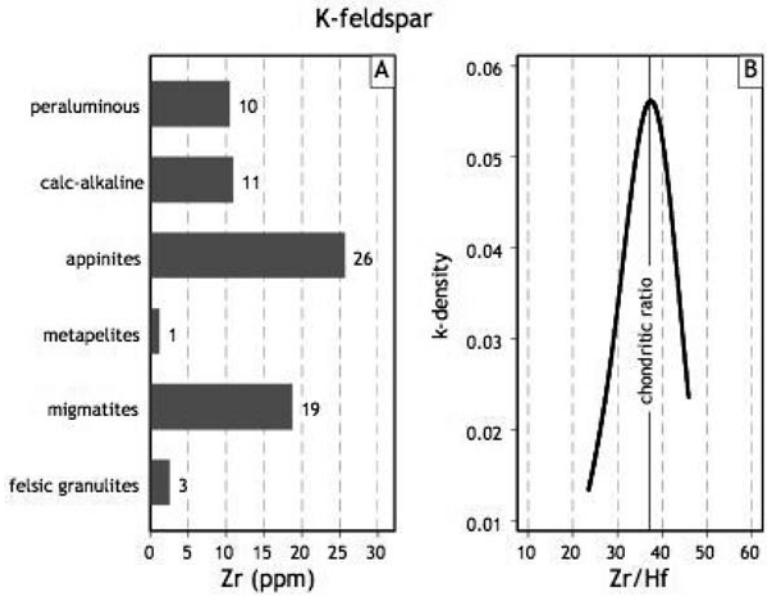

FIG. 9. A) Average concentration of Zr in K-feldspar, sorted by rock types. As in plagioclase, magmatic K-feldspar usually has detectable though highly variable amounts of Zr. Compare mode and mean values in Table 1. B) Distribution of Zr/Hf values in K-feldspar with Hf above 0.1%. Note that it coincides with the chondritic value.

a mean at 26 ppm. The K-feldspar from migmatites also has an elevated Zr content, and yields a near-symmetrical distribution with a mode at 13 ppm and a mean at 19 ppm. Lastly, most K-feldspar grains from metapelites and felsic granulites contain near-zero Zr, but outliers with a few tens of ppm are common, especially in granulites. As in plagioclase, Zr/Hf in K-feldspar with Hf > 0.1 ppm is close to the chondritic value (Fig. 9B).

Titanite

Titanite in this study contains between a few hundred to a few thousand ppm Zr. The highest values were found in grains from alkaline gabbro (mean = 2103 ppm, mode = 1550 ppm) and calc-alkaline gabbro and diorite (mean = 2023 ppm, mode = 1970 ppm) (Table 1, Fig. 10A). As observed with amphibole, titanite from the more felsic calc-alkaline rocks, tonalite, granodiorite and granite, have less Zr, with a mean of 893 ppm and a mode of 610 ppm. Remarkably, in the appinitic rocks of Iberia, where textural evidence indicates that titanite is a late mineral, probably arising by reaction between kaersutite and liquid, the concentration of Zr is much lower, with a mean of 33 ppm and a mode of 27 ppm. The value of Zr/Hf in titanite is consistently close to 15 (Fig. 10B), the lowest among rock-forming minerals, which reflects the compatibility of Hf in this mineral.

Apatite

The concentration of Zr in apatite is invariably very low (Table 1). The highest values are found in peraluminous granites (Fig. 11A); it is probable, however, that values higher than 10 ppm might result from micrometric inclusions of xenotime in apatite, as suggested by the good correspondence between Zr and Y spikes in the time-resolved signals shown by these analyses. Apatite from calc-alkaline (mean = 2.5 ppm, mode = 1.1 ppm) and alkaline rocks (mean = 3.3, mode = 1.3 ppm) rarely have Zr higher than 2–3 ppm. The same is true of apatite from leucosomes of metapelitic migmatites. The Zr/Hf value of apatite clusters around 38 (Fig. 11B).

Epidote

The concentration of Zr in magmatic epidote in calc-alkaline granitic rocks in this study is invariably low, with a mean of 5.9 ppm and a mode of 4.9 ppm (Table 1). The Zr/Hf value clusters around 20.

Rutile

This mineral commonly contains more than 100 ppm Zr (Table 1; see also Zack *et al*. 2002). In this study, the

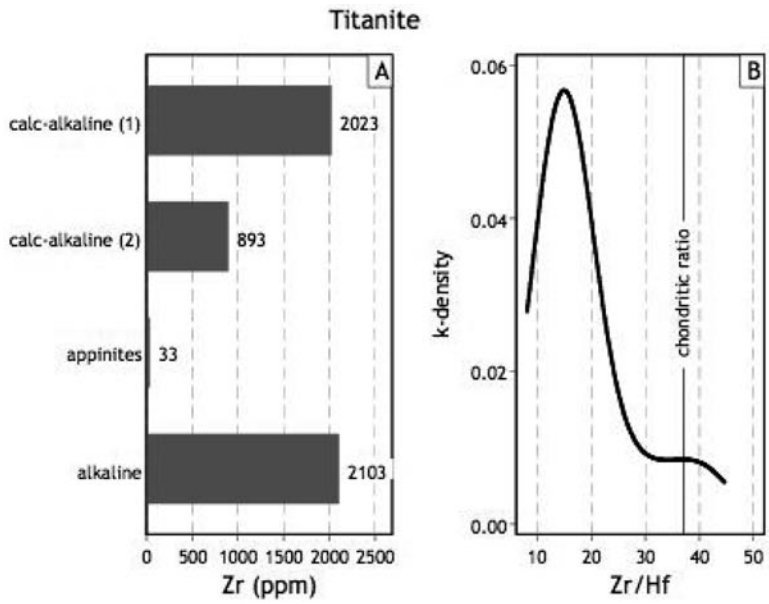

FIG. 10. A) Average concentration of Zr in titanite, sorted by rock types. Calc-alkaline (1) represents titanite from gabbro and diorite; calc-alkaline (2) represents titanite from tonalite to granite. The low concentration in titanite from appinitic rocks might be related to the late-magmatic origin of titanite in these rocks. B) Distribution of Zr/Hf values in titanite. Note that it is the lowest among rock-forming minerals.

highest concentrations were found in felsic granulites (mean = 234 ppm), and the lowest, in mafic granulites (mean = 123 ppm) and eclogites (mean = 139 ppm). The Zr/Hf value clusters around 23.

Ilmenite and magnetite

It was difficult to get reliable analyses of ilmenite and magnetite for Zr and Hf because in addition to the analytical problems mentioned in the methods section, these minerals are almost invariably too fine grained.

Ilmenite can have high Zr contents. Pearce (1990), for example, reported concentrations of Zr in ilmenite from mafic alkaline rocks as high as 3850 ppm. Bingen *et al.* (2001) showed how ilmenite is the source of Zr during high-grade metamorphism of mafic rocks, and Jang & Naslund (2003) determined an average of 485 ppm with Zr/Hf = 36 in the Skaergaard intrusion. The analyses obtained in this work (Table 1, Fig. 12A) indicate that Zr in ilmenite decreases dramatically with the silica content of the rock. Whereas calc-alkaline gabbro and diorite yielded ilmenite with a mean of 677 ppm, related tonalite and granodiorite yielded ilmenite with 105 ppm. In peraluminous granites and migmatites, ilmenite seems to have notably lower Zr, with a mean around 28–30 ppm. The Zr:Hf ratio clusters around 37–40 (Fig. 12B) and is, therefore, similar to the chondritic ratio.

Magnetite generally contains less Zr than ilmenite and has a similar Zr/Hf (Table 1). That from samples of alkali gabbro yielded an average of 47 ppm, whereas calc-alkaline granitic rocks yielded 7 ppm. The Zr/Hf value clusters around 31.

Monazite

The concentration of Zr in monazite analyzed in this study is, in most cases, below 10 ppm. The distribution is highly asymmetrical, with a mode at 0.8 ppm and a mean at 4.5 ppm (Table 1). As the highest values were mostly found in monazite from xenotime-bearing rocks, we suggest that they may result from inclusions of that mineral, so that the actual concentration of Zr in monazite is probably below 1 ppm.

Allanite

Primary allanite in this study contains elevated, but highly variable, Zr. The average of our determinations from all rock types is 135 ppm (Table 1), but values up to 400 ppm are common. The Zr/Hf value is higher than the chondritic value and clusters around 61.

Xenotime

Zircon and xenotime are isotypic, so that each may accommodate elevated concentrations of the other cation, thus forming intermediate zircon–xenotime phases (*e.g.,* Bea 1996). For this reason, xenotime [in

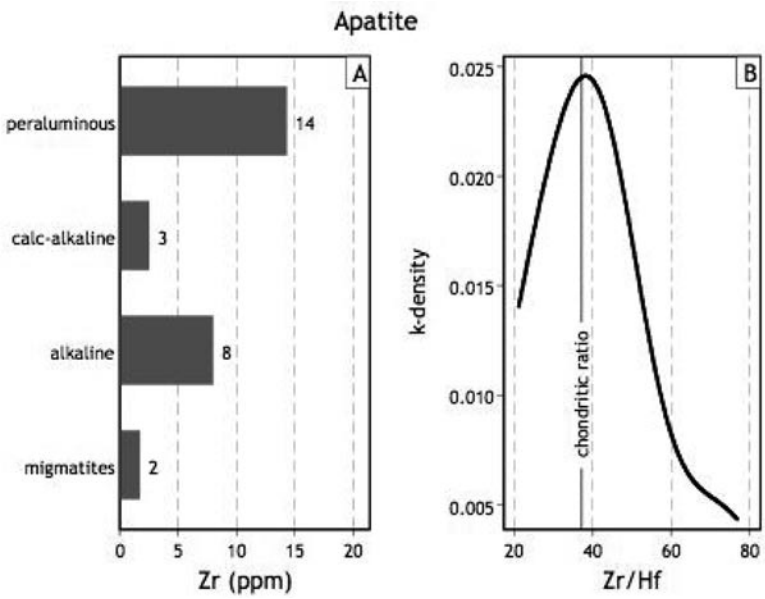

FIG. 11. A) Average concentration of Zr in apatite, sorted by rock types. B) Distribution of Zr/Hf values in apatite. The most commonly encountered value is close to the chondritic value.

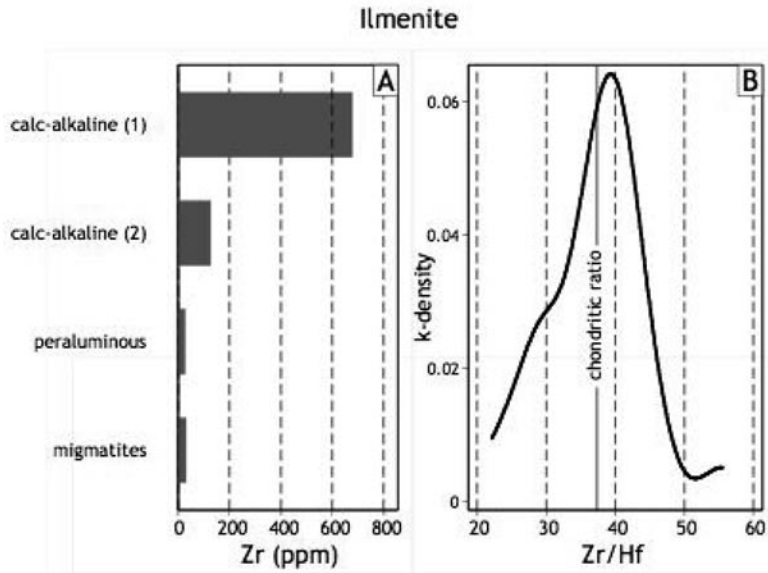

FIG. 12. A) Average concentration of Zr in ilmenite, sorted by rock types. B) Distribution of Zr/Hf values in apatite. The most commonly encountered is close to the chondritic value.

all cases xenotime-(Y)] has a highly variable level of Zr, with most determinations in this study between 0.05 wt.% and 20 wt.%. The Zr/Hf value is almost identical to that in zircon, clustering around 45.

Zircon

As would be expected, the concentration of Zr in zircon is, in general, quite constant, close to the stoichiometric value of 49.76%. The average of 511 determinations on zircon grains from a wide variety of igneous and metamorphic rocks is 49.07%; significantly lower values were found only in strongly metamict grains, owing to the presence of H_2O, and in grains with an elevated fraction of dissolved hafnon or xenotime. Values of Zr/Hf in this study vary between 20 and 70, with the most commonly encountered value at 47 (Fig. 13), which is notably higher than the chondritic value. Values below 20 are mostly found in zircon from highly fractionated segregations, especially from peraluminous magmas.

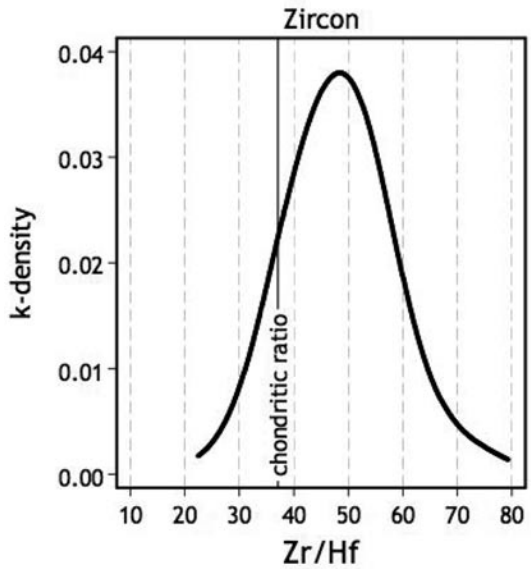

FIG. 13. Kernel-density plot of Zr/Hf in 511 zircon grains from a wide variety of igneous rocks from the Urals and Iberia. Note how the most commonly encountered value is around 47, notably higher than the chondritic value.

DISCUSSION: IMPLICATIONS OF Zr PARTITIONING IN MAJOR MINERALS

Influence on zircon saturation in melts

In their experimental model relating the concentration of Zr in a melt equilibrated with zircon to the major-element composition and temperature of the melt,

Watson & Harrison (1983) (hereafter WH) assumed that Zr is accommodated only by zircon. To understand how the partitioning of this element in other phases may affect the WH model, we will consider the following.

During partial melting of a zircon-bearing protolith, the formation of a Zr-bearing phase does not necessarily have to influence the Zr concentration in the melt. The melt provides a vehicle for Zr transport from zircon to the newly formed phase, but it will hold Zr concentration at the zircon-saturation level predicted by the WH model as long as enough zircon is available for dissolution. The formation of a Zr-bearing phase before melt segregation will accelerate the disappearance of zircon from the protolith and, once the melt is segregated, will enhance the dissolution of inherited zircon. To keep the melt at zircon-saturation level, the precipitation of 1 wt.% of garnet (50 ppm Zr), amphibole (150 ppm Zr) or titanite (2000 ppm Zr) would require the dissolution of 0.0001 wt.%, 0.0003 wt.% and 0.004 wt.% of zircon respectively, figures that gain relevance if one considers that the modal fraction of zircon in most crustal rocks is rarely higher than 0.05–0.07% (~250–350 ppm Zr). Since the major minerals that are most enriched in Zr are amphibole and titanite, this effect would result in metaluminous magmas having less zircon inheritance than peraluminous magmas if they were derived from protoliths with equal zircon contents at similar temperatures.

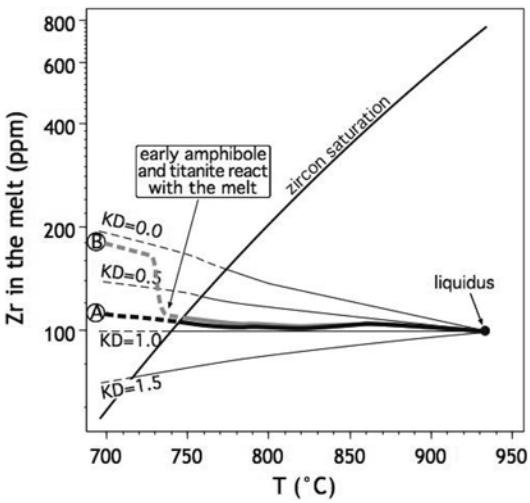

FIG. 14. Simulation of the evolution of the concentration of Zr in a metaluminous granodioritic melt. The modal composition of the precipitate and the major-element composition of the residual liquid with decreasing temperature were calculated with the software MELTS (Asimow & Ghiorso 1998, Ghiorso *et al*. 2002); see the text for details. The zircon-saturation curve was calculated from the above data and the Watson & Harrison (1983) model. K_D curves were calculated with the trace-element fractionation equation for fractional crystallization and the indicated bulk-partition coefficients (K_D); the curve $K_D = 0$ represents the absence of Zr-bearing major phases. The curve A represents the evolution of the bulk partition-coefficient calculated from the modal composition of the precipitate, as provided by MELTS, and the following Zr mineral/melt partition coefficients: $K_D^{amp/melt} = 0.5$, $K_D^{cpx/melt} = 0.25$, $K_D^{ttn/melt} = 10$, $K_D^{grt/melt} = 0.15$, estimated by assuming a $K_D^{amp/melt} = 0.5$, the central value of the amphibole rim – melt concentration ratios determined by Sisson (1994) on calc-alkaline compositions, and the average Zr concentration ratios between coexisting amphibole, clinopyroxene, and titanite of the Main Series of Stepninsk pluton (Bea *et al*. 2005), as determined in this work.

The temperature obtained with the WH model for the specific composition of a given rock (assuming it matches the composition of the liquid, which rarely happens) is known as the zircon-saturation temperature (ZST) for that rock. Though the ZST is not a real geothermometer, when applied to granitic rocks, it may be regarded as a useful estimate of the temperature of the magma at the source (*e.g.*, Hanchar & Watson 2003, Miller *et al*. 2003). How the presence of Zr-bearing phases other than zircon affects the calculation of the ZST will depend on the Zr concentration and modal fraction of these phases. Looking at Table 1, it is evident that the Zr-bearing phases of peraluminous rocks, namely garnet and perhaps the feldspars, will have negligible effects. In metaluminous rocks, on the other hand, the crystallization of titanite and amphibole may result in slightly elevated zircon-saturation temperatures. For example, the precipitation of 10% amphibole (150 ppm Zr) and 1% titanite (2000 ppm Zr) could increase the concentration of Zr in the rock by ~50 ppm above the zircon-saturation level, but this only represents an increment of the ZST of ~20°C.

Notably, the uptake of Zr by crystallizing major minerals may have a great influence on the morphology and modal abundance of zircon formed during magmatic crystallization. To illustrate this, let us consider the following example of crystallization of a metaluminous granodioritic magma (Fig. 14) modeled with the MELTS software (Ghiorso & Sack 1995, Asimow & Ghiorso 1998). The input for MELTS was as follows: (1) Magma composition: SiO_2 = 61.34%, TiO_2 = 1.09%, Al_2O_3 = 16.13%, Fe_2O_3 = 0.9%, FeO = 3.88%, MgO = 1.93%, CaO = 4.16%, Na_2O = 3.46%, K_2O = 2.67%, H_2O = 4.55 %; this corresponds to the initial magma inferred for the Stepninsk Pluton of the Uralides (Bea *et al*. 2005), for which the Zr partitioning among major minerals was determined in this work. (2) Temperature: from 945°C (liquidus) down to 655°C in intervals of 10°C. (3) Pressure: 5 kbar. (4) The $f(O_2)$ constraint: Qtz–Fa–Mgt; (5) Solid phases allowed to precipitate: titanite, amphibole, hornblende, biotite, muscovite, feldspar, quartz, "ortho-oxide", and apatite (corresponding to the modal mineralogy of Stepninsk).

The detailed MELTS output is available from the authors upon request.

Applying the WH expression to the liquid composition for each crystallization interval, as provided by MELTS, the zircon-saturation curve was first calculated. Then, assuming 100 ppm as the initial Zr concentration of the melt, and using the MELTS output and the trace-element fractionation equation for Rayleigh crystallization, the evolution of the Zr concentration was computed in fractionated liquids as a function of the temperature. These calculations were done for Zr bulk solid–melt partition coefficients (K_D) equal to 0 (no Zr-bearing phases), 0.5, 1 and 1.5, and for the K_D resulting from the modal fraction of minerals in the precipitate, provided by MELTS, and the following Zr mineral–melt partition coefficients: $K_D^{amp/melt} = 0.5$, $K_D^{cpx/melt} = 0.25$, $K_D^{ttn/melt} = 10$, $K_D^{grt/melt} = 0.15$. These were estimated by assuming a $K_D^{amp/melt} = 0.5$, the central value of the amphibole rim / melt concentration ratios determined by Sisson (1994) on calc-alkaline compositions, and the average Zr concentration ratios among coexisting amphibole, clinopyroxene, and titanite of the Main Series of Stepninsk pluton, as determined in this work.

Figure 14 shows the results of this simulation; it is evident that the crystallization of the Zr-bearing phases in the proportions foreseen by MELTS (curve A) will cause the liquid to saturate in zircon at a temperature 30°C lower than when the precipitate is formed by Zr-free minerals ($K_D = 0$) and, significantly, the amount of Zr available for zircon will be about 33% less. Besides the obvious effect of decreasing the modal fraction of this mineral, this effect would probably lead to a zircon population composed of smaller grains owing to the well-known effects of decreasing temperature on nucleation and growing rates (Kirkpatrick 1981).

TABLE 2. MOST FREQUENT VALUES (MODES) OF Zr/Hf IN MINERALS AND ESTIMATED Zr/Hf PARTITION-COEFFICIENT RATIOS*

	Zr/Hf mode	K_D^{Hf}/K_D^{Zr} calculated	K_D^{Hf}/K_D^{Zr} experimental
titanite	15	2.5	2.5
orthopyroxene	19	2	
epidote	22	1.7	
rutile	23	1.7	
amphibole	21	1.7	1.5-2
clinopyroxene	21	1.7	1.7-2.5
ilmenite	38.5	1	
apatite	38	1	
K-feldspar	36	1	
magnetite	39	0.95	1
plagioclase	40	0.9	
xenotime	45	0.8	
zircon	47	0.8	
garnet	51	0.7	0.44-1.33
allanite	61	0.6	

* The assumption is that these minerals are derived from material with a bulk Zr/Hf equal to the chondritic ratio 37.1 (McDonough & Sun 1995).

An interesting situation, represented by curve B in Figure 14, occurs where early-formed Zr-bearing minerals react with late liquids to produce Zr-free phases, for example the transformation of amphibole to biotite and the resorption of early titanite. The Zr accommodated in these minerals is released to the melt, which may then become locally oversaturated. Depending on the environment, this may lead either to overgrowths or to a new generation of zircon. The opposite situation will occur where a Zr-poor phase, such as olivine or orthopyroxene, reacts with the melt to form amphibole. If zircon was already precipitating, the partitioning of Zr into the newly formed amphibole will decrease the concentration of Zr to subsaturation and so may lead to the resorption of zircon crystals. The complex interplay among melt, Zr-bearing major silicates and zircon may be one of the main causes of the appearance of texturally discordant zones, apparently diachronous, commonly found in magmatic zircon (*e.g.,* Corfu *et al.* 2003).

Applications to the ratio Zr/Hf during petrogenetic processes

The K_D^{Hf}/K_D^{Zr} value for each mineral can be estimated from its Zr/Hf mode (Table 1) assuming a chondritic ratio (Zr/Hf = 37.1; McDonough & Sun 1995) for the magmas (or the bulk rock in the case of metamorphic minerals) from which they were derived. The resulting values (Table 2) almost exactly match the data for the few minerals already experimentally studied (see summary in Linnen & Keppler 2002). For this reason, the whole dataset in Table 2 can confidently be used for calculating the effect of Zr-bearing minerals on Zr/Hf during petrogenetic processes.

The minerals with the highest partition-coefficient of Hf relative to Zr are titanite ($K_D^{Hf}/K_D^{Zr} = 2.5$), orthopyroxene (2.0), amphibole and clinopyroxene (1.8), and epidote and rutile (1.6–1.7). Ilmenite, magnetite, the feldspars and apatite have K_D^{Hf}/K_D^{Zr} approximately equal to 1. Values less than one were found in xenotime and zircon (0.8), garnet (0.7), and allanite (0.6). Also considering the modal abundance and concentration of Zr in these minerals, it follows that the best candidates to have a strong influence on Zr/Hf are, in the order, zircon, titanite, amphibole, clinopyroxene and garnet; the influence of the other minerals would be negligible in most cases.

Figure 15 shows how the joint crystallization of zircon plus each of the aforementioned minerals affects Zr/Hf in residual melts. The effects of major minerals were simulated with the equation describing the trace-element fractionation for fractional crystallization, assuming Zr/Hf = 37.1 and 100 ppm Zr; the K_D^{Zr} values are average estimates from the literature; the K_D^{Hf} were calculated from these and the K_D^{Hf}/K_D^{Zr} shown in Table 2. The effects of zircon were simply calculated by subtracting Zr and Hf from the melt in the proportion

47:1 according to the amount of zircon crystallized. The curves for each mineral represent different zircon: mineral modal ratios.

The calculation reveals that the most effective mineral to cause higher-than-chondrite Zr/Hf values in fractionates is titanite, followed by amphibole and clinopyroxene. Nevertheless, the effects of these minerals can be easily compensated by zircon. Clinopyroxene and amphibole require a zircon:mineral modal ratio as low as 0.0002 to 0.0003, but titanite requires a modal ratio of about 0.01 (Fig. 16). Garnet fractionation, on the other hand, has little effect; the crystallization of 40 wt.% modal garnet moves Zr/Hf from 37.1 to ~ 35. These results do not change very much if the calculations are done for higher concentrations of Zr in the initial magma or reasonably different partition-coefficients for Zr.

It seems, therefore, that clinopyroxene or amphibole fractionation can increase Zr/Hf in fractionates only where the precipitation of zircon is inhibited or kept to a minimum. The most favorable situation occurs in mafic alkaline magmas, owing to their low Si and high Na activities; a striking example, shown in Figure 16A, is displayed by the camptonitic lamprophyres of central Iberia (Scarrow *et al.*, submitted). These have about 300 ppm Zr but contain very little, if any, zircon or other Zr-saturated accessory phase, so that the fractionation was caused first by titanian augite + kaersutite and then by kaersutite alone. This caused the smooth increase of Zr/Hf from 37 to 50 with a slope change at SiO_2 ± 48 coinciding with the disappearance of titanian augite phenocrysts.

The fractionation of titanite, commonly accompanied by amphibole, might be an effective way of increasing

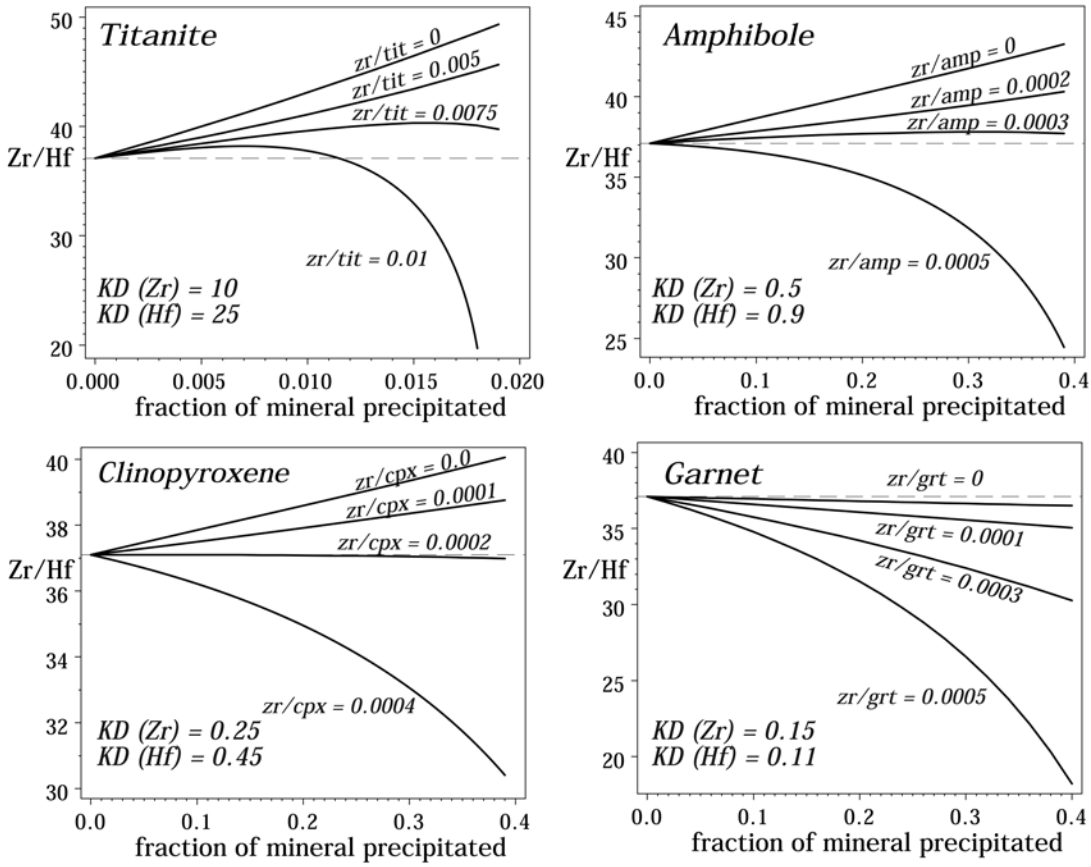

FIG. 15. Numerical simulation of the effects of the simultaneous crystallization of zircon and one Zr-bearing major phase on the Zr:Hf ratio of fractionated melts. The effects of major minerals were calculated with the trace-element fractionation equation for fractional crystallization. The K_D^{Zr} are average estimates from the literature; the K_D^{Hf} were calculated from these and the Zr :Hf partition coefficient ratios shown in Table 2. The effects of zircon were calculated by subtraction of Zr and Hf (47:1) according to the amount of zircon crystallized. The curves for each mineral represent different zircon:mineral modal ratios. Note the small proportion of zircon required to compensate the effects of amphibole and clinopyroxene.

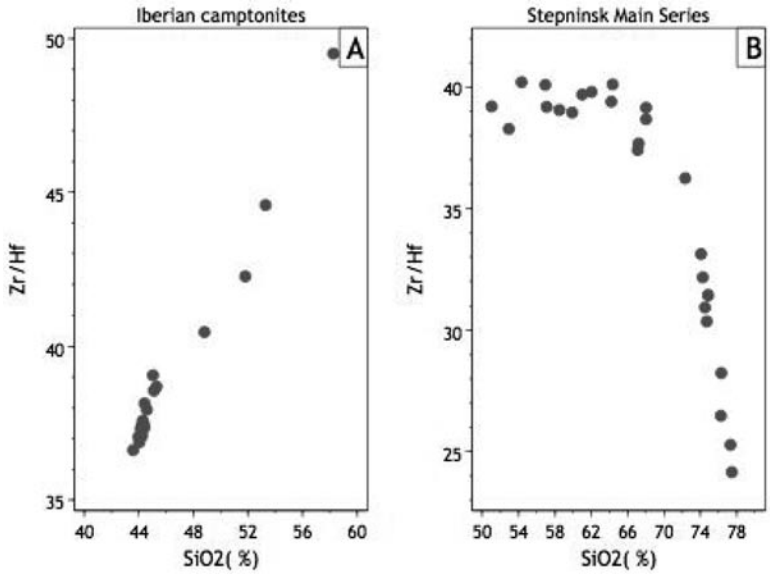

FIG. 16. Evolution of Zr/Hf in two differentiated series. A) Camptonitic lamprophyres from central Spain; Zr/Hf increases owing to zircon-absent fractionation of titanian augite + kaersutite. The slope change at $SiO_2 \approx 48$ corresponds to the disappearance of titanian augite. B) Main Series of the Stepninsk pluton. The fractionation of titanite + amphibole is compensated by zircon up to $SiO_2 \approx 68\%$, when these minerals stop crystallizing. Then, zircon fractionation dominates the system and quickly reduces Zr/Hf from 36 to 24.

Zr/Hf in fractionates, but this rarely occurs without the precipitation of sufficient zircon to compensate, or even reverse, the trend. A good example is displayed by the above-mentioned Stepninsk Pluton in the South Urals, Russia (Bea *et al*. 2005), composed of gabbro-diorite to leucogranite forming a continuous differentiation series. Here, despite strong fractionation of amphibole + titanite, the Zr/Hf ratio remains "noisily" around 38 during differentiation from gabbro-diorite ($SiO_2 \approx 52\%$) to granodiorites ($SiO_2 \approx 68\%$), compensated by zircon fractionation. In more evolved compositions, amphibole was totally replaced by biotite, and titanite stopped crystallizing, so that the only phase fractionating Zr and Hf was zircon, thus causing the rapid decrease of Zr/Hf from ~ 36 to ~ 24 (Fig. 16B).

These calculations also reveal that the most effective way for magmas to get lower-than-chondrite values of Zr/Hf in magmas is zircon fractionation, thus supporting the conclusions of Linnen & Keppler (2002). Neither garnet, owing to its low concentrations of Zr, nor xenotime or allanite, owing to low modal fraction and late crystallization, seem capable of producing perceptible differences in Zr/Hf during magmatic evolution (Fig. 15). Zircon fractionation, however, does not invariably lead to lower-than-chondrite Zr/Hf fractionates (*e.g.,* Dostal & Chatterjee 2000), though this seems to be the most common case in silicic metaluminous and peraluminous melts.

Applications to geochronology

A mineral reaction in which the reactants contain more Zr than can be accommodated in the products would also produce a Zr-rich accessory as a mass-balancing phase. The same applies to Y, REE or any other trace element that, being an essential structural component of an accessory, is also partitioned in major minerals (*e.g.,* Pan 1997). Dating the so-formed accessory phases dates the reaction that formed them, permitting high-resolution geochronology. Examples have been documented by Fraser *et al*. (1997) and Degeling *et al*. (2001), who found new zircon formed during the retrogression of Zr-bearing granulitic garnet to a Zr-free assemblage, and Bingen *et al*. (2001), who found baddeleyite, srilankite ($[Ti,Zr]O_2$) and zircon formed after Zr-rich ilmenite in mafic granulites.

Two additional examples were found in the sample collection investigated here: the formation of xenotime, instead of zircon, as a product of garnet retrogression in amphibolite-grade migmatites, and the overgrowth of new rims over zircon grains included in Zr-rich K-feldspar megacrysts.

The first process was identified in the Peña Negra migmatites, where the scarce crystals of garnet are usually rimmed by well-developed cordierite + biotite + quartz coronas (Pereira & Bea 1994), probably developed by the reaction K-feldspar + garnet + melt = biotite + cordierite + quartz (Thompson 1982). Garnet has about 500 ppm Y, 250 ppm HREE, 250 ppm P, and 56 ppm Zr, whereas the retrogression products, cordierite, biotite and quartz, have negligible amounts of all these elements (Table 3). The coronas (Fig. 17) contain no zircon, but abundant small grains of xenotime ([Y,HREE]PO_4), a mineral that never appears included in garnet and is uncommon, but still found, in other areas of the same thin section. Xenotime instead of zircon, therefore, seems to be the mass-balancing accessory of the reaction. This can be easily understood because in the trace-element leftover after garnet breakdown, Y+ HREE are far more abundant than Zr, and there is enough P to precipitate all Y+ HREE as a phosphate. In addition, xenotime, which forms a solid solution with zircon (Vlasov 1966), will dissolve the small fraction of $ZrSiO_4$ formed during the reaction, inhibiting the formation of zircon as an independent phase. This mechanism is reflected by the fact that xenotime from the retrogression coronas is notably richer in Zr, but poorer in Th and U, than xenotime from other areas (Table 3). A simple mass-balance indicates that the volume ratio garnet/xenotime is about 1000, *i.e.,* about 1% of the area formerly occupied by garnet in thin section, roughly about 0.3–0.5% of the corona, may currently be occupied by xenotime. These figures are in good agreement with the relative modal proportions found in thin sections (*e.g.,* Fig. 17A).

The formation of either xenotime or zircon during the retrogression of garnet will depend on the trace-element composition of the garnet. In metapelites, the concentration of Y, HREE and P in garnet decreases with increasing metamorphic grade (Bea *et al.* 1997, Bea & Montero 1999, and unpublished data). It seems, therefore, that the breakdown of amphibolite-grade garnet would tend to form xenotime, as in the Peña Negra migmatites, whereas the breakdown of granulite-grade garnet would tend to form zircon, as documented by Fraser *et al.* (1997) and Degeling *et al.* (2001). Xenotime is also useful for radiometric dating (Fletcher *et al.* 2004), so that this difference does not affect the potential of garnet-breakdown reactions for geochronology. But the formation of either zircon or xenotime by this mechanism is probably limited to metapelites. The retrogression of garnet from eclogites or mafic granulites hardly requires a mass-balancing accessory because it contains little Zr (Y and HREE) (Table 1) and other Zr–Y–HREE-bearing phases, such as amphibole, frequently appear as products of the reaction. As noted by Bingen *et al.* (2001), reactions involving Zr-rich ilmenite are much more promising for these rocks.

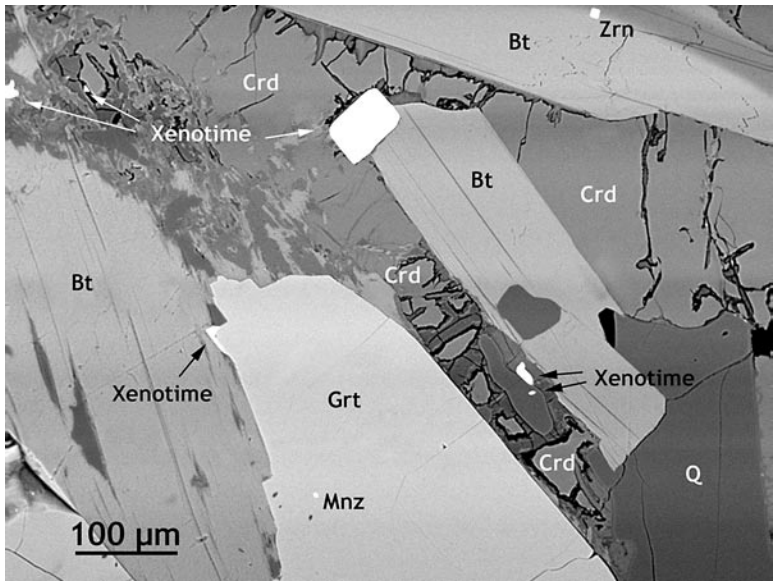

FIG. 17. SEM image of the retrogession aureole of a garnet from a metapelite migmatized at amphibolite-grade conditions. Qtz: quartz; Crd: cordierite; Grt: garnet; Bt: biotite; Mnz: monazite, The mass-balancing accessory product of the reaction is Zr-rich xenotime rather than zircon.

TABLE 3. LEVELS OF CONCENTRATION OF SELECTED ELEMENTS IN MINERALS IN THE GARNET-RETROGRESSION CORONA SHOWN IN FIGURE 17

	Garnet (n = 10)		Cordierite (n = 14)		Biotite (n =11)		Xenotime A (n = 3)		Xenotime B (n = 2)	
	mean	σ	mean	σ	mean	σ	mean	σ	mean	σ
P	253	26	28	10	41	14	13.1×10^4	0.14×10^4	13.4×10^4	0.13×10^4
Y	498	129	0.05	0.08	0.03	0.03	34.6×10^4	0.68×10^4	35.9×10^4	0.1×10^4
HREE	244	32	0.04	0.08	0.01	--	17.2×10^4	0.59×10^4	17.9×10^4	0.1×10^4
Zr	56	18	0.16	0.18	0.47	0.33	1.9×10^4	1.6×10^4	639	428
Th	0.01	0.01	0.02	0.03	<0.01	--	233	121	995	103
U	0.04	0.05	0.06	0.2	<0.01	--	569	179	3190	614

Xenotime A is a product of the reaction. Xenotime B represent the rare grains from the same section found far from garnet coronas. Compared to xenotime, garnet has P in excess over Y and HREE. Note how xenotime A is richer in Zr, but poorer in Th and U, than xenotime B.

Another zircon-forming reaction is the transformation of Zr-rich feldspars to Zr-free feldspars plus zircon. This phenomenon is well represented in a volcaniclastic formation of central Iberia, the Ollo de Sapo (Frog's Eye) Formation (Diaz Montes *et al.* 2004), a felsic gneiss with huge (up to 10 cm) megacrysts of K-feldspar of magmatic origin within a medium- to fine-grained groundmass. The megacrysts have variable and irregularly distributed Zr, from 0 to 30 ppm, and scattered inclusions of zircon. Some, but not all, inclusions show a low-U rim with a marked zonal structure and variable thickness (Fig. 18). Rim morphology suggests highly different growth-rates over the same face of the inclusion, exactly what one would expect if the diffusion of Zr toward the inclusion had been channeled through favorable structures (cracks, microveins, *etc.*) of the host crystal. Ongoing U–Pb ion-microprobe and LA–ICP–MS dating reveals that whereas the cores yielded ages clustering around 490–485 Ma, the probable age of the Ollo de Sapo Formation, the rims yielded abnormal ages of 460–420 Ma, younger than the minimum stratigraphic age of the formation, which is well known because it is discordantly overlain by the Arenig (488–478 Ma) Armorican Quartzite. Zircon grains separated from the groundmass, on the other hand, neither show rims with comparable morphology nor yielded U–Pb ages younger than 485 Ma. It seems, therefore, that the rims of younger zircon included in the Zr-rich K-feldspar megacrysts grew at a subsolidus stage from Zr supplied by the host feldspar, although the factor that triggered the growth of the new rims is still poorly known. It could have occurred during metamorphism, deformation or simply ordering of the Zr-rich feldspar upon cooling. Once properly understood, this mechanism may provide a useful tool for tracking the post-crystallization history of magmatic rocks.

Looking at Table 1, and considering the levels of the REE in common minerals (*e.g.,* Bea 1996), it seems that other reactions could also form mass-balancing accessory phases useful for geochronology, such as zircon, xenotime and monazite. In the authors' opinion, reactions involving the transformation of amphibole to biotite in magmatic and late-magmatic systems, and the breakdown of titanite at either metamorphic or magmatic conditions, are potentially interesting and deserve further study. The knowledge of the role of accessory phases, either as reactants or products, in major mineral–mineral and mineral–melt reactions, is still in its infancy; however, it seems a promising field that can have a great impact not only on high-resolution geochronology but, presumably, also on the reaction kinetics and the stability of major phases.

Summary and Conclusions

Several rock-forming minerals contain significant concentrations of Zr and Hf (Table 1). The highest values are found in xenotime, followed by titanite, ilmenite, rutile, allanite, amphibole, clinopyroxene, garnet, magnetite and, occasionally, plagioclase, K-feldspar and orthopyroxene; Degeling *et al.* (2001) also found elevated Zr concentrations in osumilite. Olivine, cordierite, biotite, muscovite, apatite, epidote and monazite, on the other hand, have low abundances of Zr, in most cases less than 1 ppm, and those of Hf, near or below the detection limit. The partitioning of Hf relative to Zr in rock-forming minerals also shows large differences (Table 2). The highest K_D^{Hf}/K_D^{Zr} were found in titanite ($K_D^{Hf}/K_D^{Zr} = 2.5$), orthopyroxene (2.0), amphibole and clinopyroxene (1.8), and epidote and rutile (1.6–1.7). Ilmenite, magnetite, the feldspars and apatite have $K_D^{Hf}/K_D^{Zr} \approx 1$. Values less than one were

found in xenotime and zircon (0.8), garnet (0.7), and allanite (0.6). The most relevant implications of these data are as follows:

1) The growth of a Zr-bearing phase during partial melting does not influence the Zr concentration of the melt predicted by the Watson & Harrison (1983) model, but increases the amount of zircon that can be dissolved at a given temperature.

2) Before melt segregation, this will accelerate the disappearance of zircon from the protolith. In already segregated melts, it will enhance the dissolution of inherited zircon. This effect will be more marked in metaluminous magmas precipitating amphibole and titanite than in any other type of magma.

3) The effect of Zr-bearing phases on the WH zircon saturation temperature is negligible in peraluminous rocks, but can be of some importance in metaluminous rocks, increasing the calculated ZST by 20 to 30°C at most.

4) The uptake of Zr by crystallizing major minerals influences the morphology and modal abundance of magmatic zircon. The crystallization and resorption of Zr-bearing major silicates affect the growth of magmatic zircon, and may be one of the main causes of the appearance of texturally discordant zones, apparently diachronous, commonly found in this mineral.

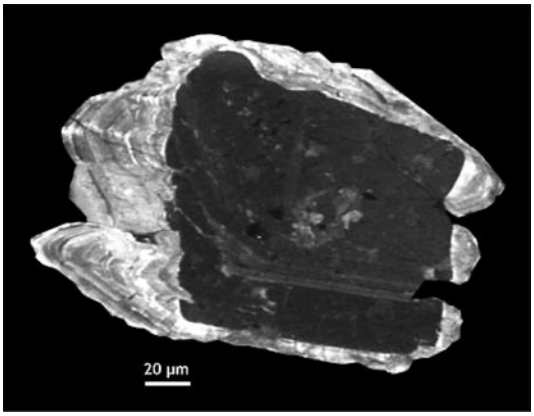

FIG. 18. Cathodoluminescence image of a zircon included in a Zr-bearing K-feldspar megacryst of the volcaniclastic Ollo de Sapo Formation, Spain. The highly luminescent rim (owing to low U) yielded a U–Pb (LA–ICP–MS) age of 420 Ma, younger than the minimum stratigraphic age of the Formation, which is covered by Arenig (488–478 Ma) sediments. The core, however, yielded 490 Ma, close to real age of the Ollo de Sapo Formation (unpubl. data). The rim morphology suggests highly different growth-rates over the same face of the inclusion; the diffusion of Zr to the inclusion was presumably channelized through favorable structures (cracks, microveins, *etc*.) of the host crystal. These features indicate it grew in subsolidus conditions from Zr released by the feldspar.

5) A higher-than-chondrite Zr/Hf value in a melt can be caused by fractionation of titanite, amphibole or clinopyroxene, but this only if the precipitation of zircon is inhibited or kept to a minimum. On the other hand, the most effective way for a magma to get a lower-than-chondrite Zr/Hf value is to fractionate zircon.

In addition, we found two new examples of reactions that produce a mass-balancing accessory useful for geochronology: the formation of xenotime as a product of garnet retrogression in amphibolite-grade migmatites, and the overgrowth of new rims on zircon grains included in Zr-rich K-feldspar megacrysts.

The formation of xenotime instead of zircon occurs because in the trace-element leftover after garnet breakdown, Y+ HREE are far more abundant than Zr, and there is enough P to precipitate all Y+ HREE as xenotime. In metapelites, the formation of either xenotime or zircon depends on the trace-element budget of garnet, which is related to metamorphic grade (Bea *et al*. 1997, Bea & Montero 1999). Amphibolite-grade garnet would tend to form xenotime, whereas granulite-grade garnet would tend to form zircon. Garnet from mafic granulites and eclogites, on the other hand, can hardly be expected to form either xenotime or zircon.

The growth of new rims over zircon grains included in Zr-rich K-feldspar megacrysts was found in a felsic gneiss. These rims yield U–Pb ages younger than the minimum stratigraphic age of the gneiss, and their morphology suggests growth owing to Zr released by the feldspar and channeled to the inclusion through cracks, microveins, *etc*. in the host crystal. This mechanism, once properly understood, may provide a useful tool for tracking the post-crystallization history of magmatic rocks.

Other potentially interesting reactions deserving study are the transformation of amphibole to biotite in magmatic and late-magmatic systems, and the breakdown of titanite at either metamorphic or magmatic conditions.

ACKNOWLEDGEMENTS

The authors are greatly indebted to C.F. Miller, R. Linnen and an anonymous referee for their constructive suggestions and comments, which greatly improved the manuscript, and to O. Cazalla, J.F. Molina and J.H. Scarrow for their help during this work. J.H. Scarrow also improved the English. This project has been financially supported by the Spanish CICYT project BTE2002–04618–C02–01, and by the NATO Collaborative Grant EST–CLG–978997.

REFERENCES

ASIMOW, P.D. & GHIORSO, M.S. (1998): Algorithmic modifications extending MELTS to calculate subsolidus phase relations. *Am. Mineral.* **83**, 1127-1131.

BEA, F. (1996): Residence of REE, Y, Th and U in granites and crustal protoliths; implications for the chemistry of crustal melts. *J. Petrol.* **37**, 521-552.

BEA, F., FERSHTATER, G.B., MONTERO, P., SMIRNOV, V.N. & MOLINA, J.F. (2005): Deformation-driven differentiation of granitic magma, the Stepninsk pluton of the Uralides, Russia. *Lithos* **81**, 209-233.

BEA, F. & MONTERO, P. (1999): Behavior of accessory phases and redistribution of Zr, REE, Y, Th, and U during metamorphism and partial melting of metapelites in the lower crust, an example from the Kinzigite Formation of Ivrea–Verbano, NW Italy. *Geochim. Cosmochim. Acta* **63**, 1133-1153.

BEA, F., MONTERO, P., GARUTI, G. & ZACCARINI, F. (1997): Pressure-dependence of rare earth element distribution in amphibolite- and granulite-grade garnets. A LA–ICP–MS study. *Geostand. Newslett.* **21**, 253-270.

BEA, F., MONTERO, P. & MOLINA, J.F. (1999): Mafic precursors, peraluminous granitoids, and late lamprophyres in the Avila batholith, a model for the generation of Variscan batholiths in Iberia. *J. Geol.* **107**, 399-419.

BINGEN, B., AUSTRHEIM, H. & WESTINGHOUSE, M. (2001): Ilmenite as a source for zirconium during high-grade metamorphism? Textural evidence from the Caledonides of western Norway and implications for zircon geochronology. *J. Petrol.* **42**, 355-375.

CORFU, F., HANCHAR, J.M., HOSKIN, P.W.O. & KINNY, P.D. (2003): Atlas of zircon textures. *In* Zircon (J.M. Hanchar & P.W.O. Hoskin, eds.). *Rev. Mineral. Geochem.* **53**, 468-500.

DAVID, K., SCHIANO, P. & ALLÈGRE, C.J. (2000): Assessment of the Zr/HF fractionation in oceanic basalts and continental materials during petrogenetic processes. *Earth Planet. Sci. Lett.* **178**, 285-301.

DEGELING, H., EGGINS, S.M. & ELLIS, D.J. (2001): Zr budgets for metamorphic reactions, and the formation of zircon from garnet breakdown. *Mineral. Mag.* **65**, 749-758.

DIAZ MONTES, A., NAVIDAD, M., GONZ‡LEZ LODEIRO, F. & MART'NEZ CATAL‡N, J.R. (2004): El Ollo de Sapo. *In* Geolog'a de Espa–a. (J.A. Vera, ed.) Soc. Geol. Espa–a. & Inst. Geol. Min. Espa–a, Madrid (69-72).

DOSTAL, J. & CHATTERJEE, A.K. (2000): Contrasting behavior of Nb/Ta and Zr/Hf ratios in a peraluminous granitic pluton (Nova Scotia, Canada). *Chem. Geol.* **163**, 207-218.

FLETCHER, I.R., MCNAUGHTON, N.J., ALEINIKOFF, J.A., RASMUSSEN, B. & KAMO, S.L. (2004): Improved calibration procedures and new standards for U–Pb and Th–Pb dating of Phanerozoic xenotime by ion microprobe. *Chem. Geol.* **209**, 295-314.

FRASER, G., ELLIS, D. & EGGINS, S. (1997): Zirconium abundance in granulite-facies minerals, with implications for zircon geochronology in high-grade rocks. *Geology* **25**, 607-610.

GHIORSO, M.S., HIRSCHMANN, M.M., REINERS, P.W. & KRESS, V.C.I.I.I. (2002): A revision of MELTS aimed at improving calculation of phase relations and major element partitioning involved in partial melting of the mantle at pressures up to 3 GPa. *Geochemistry, Geophysics, Geosystems* **3**(5), 10.1029/2001GC000217.

GHIORSO, M.S. & SACK, R.O. (1995): Chemical mass transfer in magmatic processes. IV. A revised and internally consistent thermodynamic model for the interpolation and extrapolation of liquid solid equilibria in magmatic systems at elevated temperatures and pressures. *Contrib. Mineral. Petrol.* **119**, 197-212.

HANCHAR, J.M. & HOSKIN, P.W.O., eds. (2003): Zircon. *Rev. Mineral. Geochem.* **53**.

HANCHAR, J.M. & WATSON, E.B. (2003): Zircon saturation thermometry. *In* Zircon (J.M. Hanchar & P.W.O. Hoskin, eds.). *Rev. Mineral. Geochem.* **53**, 89-112.

JANG, Y.D. & NASLUND, H.R. (2003): Major and trace element variation in ilmenite in the Skaergaard Intrusion, petrologic implications. *Chem. Geol.* **193**, 109-125.

KAMBER, B.S. & COLLERSON, K.D. (2000): Zr/Nb systematics of ocean island basalts reassessed – the case for binary mixing. *J. Petrol.* **41**, 1007-1021.

KIRKPATRICK, R.J. (1981): Kinetics of crystallization of igneous rocks. *In* Kinetics of Geochemical Processes (A.C. Lasaga & R.J. Kirkpatrick, eds.). *Rev. Mineral.* **8**, 321-396.

LINNEN, R.L. (1998): The solubility of Nb–Ta–Zr–Hf–W in granitic melts with Li and Li+F, Constraints for mineralization in rare metal granites and pegmatites. *Econ. Geol.* **93**, 1013-1025.

LINNEN, R.L. & KEPPLER, H. (2002): Melt composition control of Zr/Hf fractionation in magmatic processes. *Geochim. Cosmochim. Acta* **66**, 3293-3301.

MCDONOUGH, W.F. & SUN, S.S. (1995): The composition of the Earth. *Chem. Geol.* **120**, 223-253.

MILLER, C.F., MCDOWELL, S.M. & MAPES, R.W. (2003): Hot and cold granites? Implications of zircon saturation temperatures and preservation of inheritance. *Geology* **31**, 529-532.

PAN, YUANMING (1997): Zircon- and monazite-forming metamorphic reactions at Manitouwadge, Ontario. *Can. Mineral.* **35**, 105-118.

PEARCE, N.J.G. (1990): Zirconium and niobium-bearing ilmenites from the Igaliko dyke swarm, South Greenland. *Mineral. Mag.* **54**, 585-588.

PEARCE, N.J.G., PERKINS, W.T., WESTGATE, J.A., GORTON, M.P., JACKSON, S.E., NEAL, C.R. & CHENERY, S.P. (1997): A compilation of new and published major and trace ele-

ment data for NIST SRM 610 and NIST SRM 612 glass reference materials. *Geostand. Newslett.* **21**, 115-144.

PEREIRA, M.D. & BEA, F. (1994): Cordierite-producing reactions at the Peña Negra complex, Avila batholith, central Spain. The key role of cordierite in low-pressure anatexis. *Can. Mineral.* **32**, 763-780.

SEIFERT, W. & KRAMER, W. (2003): Accessory titanite, an important carrier of zirconium in lamprophyres. *Lithos* **71**, 81-98.

SISSON, T.W. (1994): Hornblende–melt trace-element partitioning measured by ion microprobe. *Chem. Geol.* **117**, 331-344.

STATACORP. (2005): *Stata Statistical Software, Release 9*. College Station, TX, StataCorp LP.

THOMPSON, A.B. (1982): Dehydration melting of pelitic rocks and the generation of H_2O – undersaturated granitic liquids. *Am. J. Sci.* **282**, 1567-1595.

VANNUCCI, R., BOTTAZZI, P., WULFF PEDERSEN, E. & NEUMANN, E.R. (1998): Partitioning of REE, Y, Sr, Zr and Ti between clinopyroxene and silicate melts in the mantle under La Palma (Canary Islands), implications for the nature of the metasomatic agents. *Earth Planet. Sci. Lett.* **158**, 39-51.

VILLASECA, C., ROMERA, C.M., DE LA ROSA, J. & BARBERO, L. (2003): Residence and redistribution of REE, Y, Zr, Th and U during granulite-facies metamorphism, behaviour of accessory and major phases in peraluminous granulites of central Spain. *Chem. Geol.* **200**, 293-323.

VLASOV, K.A. (1966): *Geochemistry and Mineralogy of Rare Elements and Genetic Types of Their Deposits*. Israel Program for Scientific Translation, Jerusalem, Israel.

WATSON, E.B. & HARRISON, T.M. (1983): Zircon saturation revisited, temperature and composition effects in a variety of crustal magma types. *Earth Planet. Sci. Lett.* **64**, 295-304.

ZACK, T., KRONZ, A., FOLEY, S.F. & RIVERS, T. (2002): Trace element abundances in rutiles from eclogites and associated mica schist. *Chem. Geol.* **184**, 97-122.

Received October 25, 2004, revised manuscript accepted February 25, 2006.